

Force Unfolding Single RNAs: from Equilibrium to Far-from Equilibrium

Fei Liu* and Zhong-can Ou-Yang*†

*Center for Advanced Study, Tsinghua University, Beijing 100084, China and

†Institute of Theoretical Physics, The Chinese Academy of Sciences, P. O. Box 2735, Beijing 100080, China

(Dated: November 7, 2018)

We summarize the recent simulation progress of micromanipulation experiments on RNAs. Our work mainly consults with two important small RNAs unfolding experiments carried out by Bustamante group. Our results show that, in contrast to protein cases, using the single polymer elastic theory and the well known RNA secondary structure free energy knowledge, we can successively simulate various behaviors of force unfolding RNAs under different experimental setups from equilibrium to far-from equilibrium. Particularly, our simulation would be helpful in understanding Jarzynski's remarkable equality, which its experimental test has received considerable attention.

I. INTRODUCTION

Ribonucleic Acid (RNA) is now known to be involved in many biological processes, such as carriers of genetic information (messenger RNAs), simple adapters of amino acids (transfer RNAs), and enzymes catalyzing the reactions in protein synthesis, cleavage and synthesis of phosphodiester bonds (1; 2). In particular, recent discoveries indicated that a class of RNA called small RNA operates many of cell's control (for a report, see 3). These diverse and specific biological functions of RNA are guided by their unique three-dimensional folding. Therefore, prediction or measurements of RNA folding and folding dynamics becomes one of central problems in biological studies.

In addition to standard experimental methods such as X-ray crystallograph and NMR spectroscopy, single-molecule manipulation technique developed in the past decade provides a fresh and promising way in resolving the RNA folding problem (4; 5; 6; 7; 8; 9). As a concrete example, an optical tweezer setup is sketched in Fig. 1 (10; 11): a single RNA molecule is attached between two beads with RNA:DNA hybrid handle; one bead is held by a pipette, and the other is in a laser light trap¹. By moving the position of the pipette, the distance between the two beads and the force acting on the bead in the light trap can be measured with high resolution. This sophisticated setup has showed its abilities in recording the time-traces of the end-to-end distance of a small 22-basepair RNA hairpin (6), and resolving complicated unfolding pathways of 1540-base long 16S ribosomal RNA (5).

On theoretical side, although complete three-dimensional RNA folding prediction so far seems enor-

mously difficult (12), RNA structural prediction from physical point of view has made great progress on the level of secondary structure (13; 14; 15). The advent of the single-molecule experiments addresses a challenging issue for theorists: whether or how can we apply the known secondary structural RNA knowledge to explain or predict the phenomena observed in the single-molecule experiments? Under force stretching or twisting, the elastic properties which were cared little or even neglected before now must be seriously took into account.

Many theoretical efforts have been devoted to understand force unfolding RNAs (16; 17; 18; 19; 20; 21; 22). However these theories or models are too simple to be applied in experiments; useful free energy data about RNA secondary structure obtained before were often neglected. Moreover, they just studied equilibrium cases, while intriguing nonequilibrium phenomena were beyond their scopes. Simulation method should be a good choice to overcome these shortcomings. But we noted that, compared to enormous simulation works about force unfolding proteins (23; 24; 25; 26; 27), the simulations for RNAs are few (5) though biological importance of the later is the same as the former. To fill this gap, our group developed stochastic methods and applied it to investigate the interesting force unfolding single RNAs experiments (28; 29). In this paper, we will summarize our previous effort and extend them to investigate more intriguing issue, the remarkable Jarzynski's equality (30), which its experimental test has attracted considerable attention.

II. MODEL AND METHOD

A. RNA folding without force

A RNA sequence is denoted by a nucleotides string $l = (x_1, x_2, \dots, x_n)$, $x_i \in \{A, U, C, G\}$; the bases x_1 and x_n are the nucleotides at 5' and 3' end of the sequence, respectively. A secondary structure S of a RNA sequence is a list of base pairs $[x_i, x_j]$ that must satisfy two conditions: every base forms a pair with at most one other

¹ In practice, the RNA is attached between the two beads with two RNA:DNA hybrid handles. To simplify simulation method, only one handle is considered. It should not change following discussions.

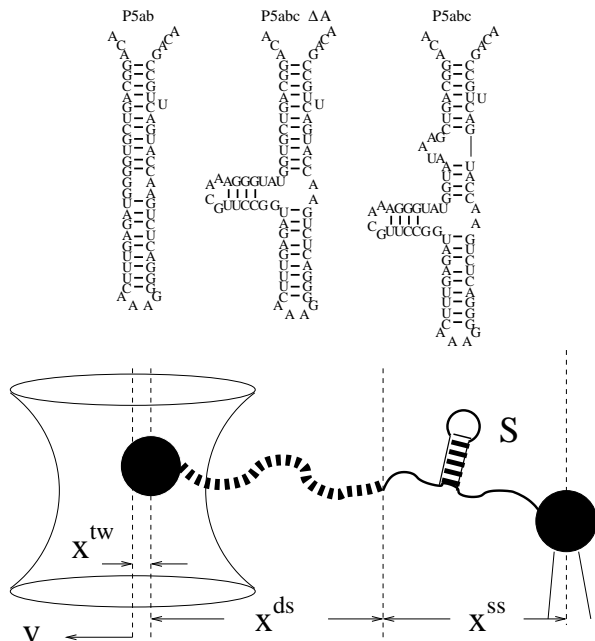


FIG. 1 Sketch of an optical tweezer setup and the RNA molecules studied in the work. We denote the region between the two arcs as the optical trap. RNA molecules are attached between the two beads (larger black points) with a RNA:DNA hybrid handle (the black dash curves). The center of the light trap is moved with velocity v . Here the total distance at time t is $z(t) = x^{tw} + x^{ds} + x^{ss}$. The individual extensions, x^{tw} the position of the bead with respect to the center of the optical trap, x^{ds} the end-to-end distance of the double-stranded DNA (dsDNA) handles, and x^{ss} The end-to-end distance of the single RNA are freely fluctuated. The RNA native structures for the three small RNA sequences, P5ab, P5abc Δ A, and P5abc are folded by Vienna Package 1.4.

base, and if any two base pairs $[x_i, x_j]$ and $[x_k, x_l]$ are in the list, then $i < k < j$ implies $i < l < j$. All structures of the sequence l comprise a set, $S(l) = \{S_0, S_1, \dots, S_m, \mathbf{0}\}$, here $\mathbf{0}$ denotes the completely open chain conformation.

In order to describe the folding or unfolding process as a time-ordered series of the structures in the set $S(l)$, a relation M which specifies whether two structures are accessible from each other by an elementary “move” must be reasonably defined. The definition is identical to specifying a metric in the set $S(l)$. Any secondary structure formation or dissolving hence can be described by a succession of elementary steps chosen according to some distributions from a pool of acceptable moves in the conformational space $C(l) = \{S(l), M\}$. In the absence of mechanical force, two kinds of move sets have been proposed in modelling secondary structural RNA folding: one is the formation or decay of a single helix (32; 33), and the other is the removal or insertion of single base pairs per time step (34; 35). We make use of the latter, for it is the simplest move set on the level of secondary structure. Moreover, we mainly focus on smaller RNAs. The formation or removal of a helix may cause larger

structural changes, while its physical relevance of RNA folding or unfolding seems debatable.

B. RNA unfolding under mechanical force

According to the difference of the external controlled parameters, the RNA unfolding experiments can be carried out under constant extension and constant force, i.e., the constant extension and the constant force ensembles (6).

We first consider the constant extension ensemble. Fig. 1 is the sketch of an optical tweezer setup for this ensemble. The position of the center of the light trap is moved according to a time-dependent relationship $z(t) = z_0 + vt$, where $z(t)$ is the distance between the centers of the light trap and the bead held by the micropipette, z_0 is offset at time $t = 0$ and v is the constant velocity. We suppose that the changes of the extensions of RNA and the handle proceed along one direction, and the physical effect of the beads is negligible. Any state of the system at time t then can be specified with three independent quantities, the extension of the RNA x^{ss} , the end-to-end distance of the handle x^{ds} , and the RNA secondary structure S , i.e., the system in i -state at time t $(S_i, x_i^{ds}, x_i^{ss})_t$. We do not include x^{tw} here for the sum of individual extensions satisfies the constraint condition, $z(t) = x^{tw} + x^{ds} + x^{ss}$. Hence, the unfolding of the single RNA proceeds in an conformational space $C(l) = S(l) \times R^{ds} \times R^{ss}$, where $R^{ds} = (0, l_{ds})$ and $R^{ss} = (0, l_{ss})$ and l_{ds} and l_{ss} are the contour lengths of the handle and the RNA molecule, respectively. In order to describe this process as a time-ordered series of the conformations in the space, a relation M which specifies whether two conformations are accessible from each other by an elementary “move” (or neighbors) must be reasonably defined. We propose the following move set (29),

$$\begin{aligned} (S_i, x_i^{ds}, x_i^{ss})_t &\rightarrow (S_j, x_i^{ds}, x_i^{ss})_{t'}, i \neq j \\ (S_i, x_i^{ds}, x_i^{ss})_t &\rightarrow (S_i, x_i^{ds} \mp \delta, x_i^{ss} \pm \delta)_{t'}, \\ (S_i, x_i^{ds}, x_i^{ss})_t &\rightarrow (S_i, x_i^{ds} \pm \delta, x_i^{ss})_{t'}. \end{aligned} \quad (1)$$

The first kind of the moves is the removal or insertion of single base pairs while fixing the extensions x^{ds} and x^{ss} . The other two kinds are to respectively move the positions of the end of the handle and the end of single-stranded RNA with a small displacement δ , while the secondary structure is fixed simultaneously.

Given the system state i at time t , the systematic energy can be written as

$$E_i(t) = \Delta G_i^0 + u(x_i^{tw}) + W^{ds}(x_i^{ds}) + W^{ss}(x_i^{ss}, n_i), \quad (2)$$

where ΔG_i^0 is the free energy obtained from folding the RNA sequence into the secondary structure S_i , and the elastic energies of the optical trap, the handle, and the single-stranded part of the RNA are

$$u(x_i^{tw}) = \frac{1}{2} k_{tw} x_i^{tw}(t)^2,$$

$$W^{ds}(x_i^{ds}) = \int_0^{x_i^{ds}} f_{ds}(x') dx', \quad (3)$$

$$W^{ss}(x_i^{ss}, n_i) = x_i^{ss} f(x_i^{ss}, n_i) - \int_0^{f(x_i^{ss}, n_i)} x_{ss}(f', n_i) df',$$

respectively, and $x_i^{tw}(t) = z(t) - x_i^{ds} - x_i^{ss}$. In the expression W^{ds} , $f_{ds}(x')$ is the average force of the handle at given extension x' ,

$$f_{ds}(x') = \frac{k_B T}{P_{ds}} \left(\frac{1}{4(1-x'/l_{ds})^2} - \frac{1}{4} + \frac{x'}{l_{ds}} \right), \quad (4)$$

and P_{ds} is the persistence length of double stranded handle. In the expression W^{ss} , $x_{ss}(f', n_i)$ is the average extension of the single stranded part of the RNA whose bases (exterior bases) are n_i at given force f' ,

$$x_{ss}(f', n_i) = n_i b_{ss} \left[\coth\left(\frac{f' P_{ss}}{k_B T}\right) - \frac{k_B T}{f' P_{ss}} \right], \quad (5)$$

where b_{ss} and P_{ss} are the monomer distance and the Kuhn length of the single-stranded RNA, respectively (10; 36). Note that $f(x_i^{ss}, n_i)$ is the inverse function of $x_{ss}(f', n_i)$, and the contour length of the RNA $l_{ss} = b_{ss} n_i$. The light trap here is simply assumed to be a harmonic potential with spring constant k_{tw} . Hence the loading rate is $r = k_{tw} v$.

In the real experiments, constant force can be imposed on RNA molecules with feedback-stabilized optical tweezers capable of maintaining a preset force by moving the beads closer or further apart. Including the feedback mechanism in theoretical study is not essential now. Therefore the energy of tweezer in Eq. 2 is replaced by $-f \times (x_i^{ss} + x_i^{ds})$.

C. Continuous time Monte Carlo algorithm

Given the move sets and the unfolding conformational spaces, the RNA unfolding for the two ensembles can be modelled as a Markov process in their respective spaces. Following conventional stochastic kinetics of chemical reactions, these processes are described as the master equation,

$$\frac{dP_i(t)}{dt} = \sum_{j=0} [P_j(t) k_{ji} - P_i(t) k_{ij}], \quad (6)$$

where $P_i(t)$ is the probability of the system being i -state at time t , and k_{ij} is the transition probability from i -state to j -state.

The form of the master equation looks relatively simple, however it is mathematically intractable to solve analytically for simple ‘‘reaction’’ system such as RNA P5ab. Previous work has demonstrated that a continuous time Monte Carlo simulation is an excellent approach toward

the stochastic process described by Eq. 6 (34; 37; 38). As a variant of the standard Monte Carlo method, the *continuous time Monte Carlo* (CTMC) method is very efficient and fast because of lacking of waiting times due to rejection. In contrast to standard MC method, instead of the MC step used to approximate the real time, the ‘‘time’’ in Gillespie’s method could be real if the transition probabilities were calculated by first principles or empirically.

The key formula in CTMC is that, given the system at i -state at current time t , the probability density $p(j, t'|i, t)$ that the next state is j and it occurs at time t' is

$$p(j, t'|i, t) = k_{ij}^{t'} \exp\left(-\int_t^{t'} \sum_l k_{il}^\tau d\tau\right), \quad (7)$$

where k_{ik}^τ are transition probabilities from the i -state to the neighbouring k -state at time τ , which can be time-dependent or time-independent (no parameters τ) (38; 39), and the sum is over all neighbors of i -state. According to Eq. 7, then the time t' for the next state to occur can be obtained by solving the following equation,

$$r_1 = \exp\left(-\int_t^{t'} \sum_l k_{il}^\tau d\tau\right), \quad (8)$$

where r_1 is a uniform random number in the interval $[0,1]$. For time-independent situation, the equation reduces to most common expression $r_1 = \exp[-(t' - t) \sum_l k_{il}]$. While if the transition probabilities involve time t , then numerical methods for integration and root finding have to be applied (40). Then the next state j is chosen if another uniform random number $r_2 \leq \sum_{l=1}^j k_{il}^{t'} / \sum_l k_{il}^{t'}$.

We assume that the transition probabilities satisfy the symmetric rule (41)

$$k_{ij}^t = \tau_o^{-1} \exp(-\beta(E_j(t) - E_i(t))/2), \quad (9)$$

where τ_o scales the time axis of the unfolding process from the experimental measurements. Apparently, the transition probabilities satisfy the detailed balance condition.

D. Partition function method in equilibrium

If the moving velocity of the light trap vanishes, an exact partition function method can calculate the molecular average extension and the average force under the given distance z (20). The method is an extension of the partition function method proposed for RNA secondary structural prediction (14). Different from the experimental measurements of the free energy with slow pulling velocity (quasi-equilibrium process) (7), we obtain the equilibrium information by this exact method. Considering coincidences of formulae and new physical quantities needed, we rewrite the formulae in Ref. (20).

The key idea of the exact method is that the partition function over all secondary structures of a given RNA can be calculated by dynamic programming (14). Given the partition function $Q(i, j, m)$ on the sequence segment $[i, j]$ with exterior bases m , its recursion formula is as follows,

$$Q(i, j, m) = \mathbf{1}\delta_{m, j-i+1} + qb(i, \Delta + j - m) + \sum_{k=i}^{j-1} \sum_{l=1}^{k-i+1} Q(i, k, l) \times qb(k+1, l + \Delta + j - m), \quad (10)$$

where $\Delta = 2$, the partition function $qb(i, j)$ on the sequence segment $[i, j]$ for which the i and j bases are paired; Vienna Package 1.4 provides the calculation codes (42).

For the constant extension ensemble, let the partition function of the RNA molecule at extension x (including the handle) be $Z_n(x)$. Then the function can be written as

$$Z_n(x) = \sum_m^n \int_0^{l_{ds}} \int_0^{m b_{ss}} dx^{ds} dx^{ss} \delta(x - x^{ds} - x^{ss}) Q(1, n, m) \exp(-\beta W(x^{ds}, x^{ss}, m)) \quad (11)$$

where $W(x^{ds}, x^{ss}, n) = W^{ds}(x^{ds}) + W^{ss}(x^{ss}, n)$. The molecular free energy landscape along x then is $G_o(x) = -\beta^{-1} \ln Z_n(x)$. To calculate the average force $\langle f \rangle$ and the average extension $\langle x \rangle$ at given distance z , the systematic partition function $\mathcal{Z}_n(z)$ required is

$$\mathcal{Z}_n(z) = \int_0^z dx Z_n(x) \exp(-\beta u(z-x)). \quad (12)$$

Then the systematic free energy $G(z) = -\beta^{-1} \ln \mathcal{Z}_n$, $\langle f \rangle = \partial G(z) / \partial z$ and $\langle x \rangle = z - \langle f \rangle / k_{tw}$.

While for the constant force ensemble, the partition function $\mathcal{Z}_n(f)$ under given force f is

$$\mathcal{Z}_n(f) = \int_0^{(l_{ds} + l_{ss})} dx Z_n(x) \exp(\beta f x), \quad (13)$$

and the average extension $\langle x \rangle = \beta^{-1} \partial \ln \mathcal{Z}_n / \partial f$.

E. Parameters and measurement

We simulate the single RNA folding and unfolding under mechanical force at the experimental temperature $T = 298K$. The elastic parameters used are: $P_{ds} = 53$ nm, $l_{ds} = 320$ nm, $b_{ss} = 0.56$ nm, $P_{ss} = 1.5$ nm, and $k_{tw} = 0.2$ pN/nm. We use the single-stranded DNA parameters for the single stranded part of RNA because they have similar chemical structure. The displacement $\delta = 0.1$ nm. The free energy parameters for the RNA secondary structures are from the Vienna package 1.4 (42) in standard salt concentrations $[Na^+] = 1$ M and $[Mg^{2+}] = 0$ M. In addition to the standard Watson-Crick base pairs (AU and CG), GU base pair is allowed in our

simulation. Formation of an isolated base pairs is forbidden because of their instability. In the constant extension ensembles, the force f_i acting on the RNA molecule at i -state is calculated by $f_i = k_{tw} x_i^{tw}$, and the bead-to-bead distance $x_i^{bb} = x_i^{ds} + x_i^{ss}$. In the constant force ensemble, the extension of the molecule is just x_i^{bb} .

III. RESULTS AND DISCUSSION

A. Single RNAs thermodynamics

A comparison between our simulation in equilibrium and the prediction of the exact partition function method should be helpful in confirming the correctness of our method. We simulate the average force-extension curves of the three RNA molecules for the two ensembles with standard approach: the average physical quantity A is calculated according to $\langle A \rangle = \tau^{-1} \int_0^\tau A(t) dt$, here $\tau = 10^6$; see Fig. 2. The force-extension curves calculated by the exact method are plotted with different kinds of curves. We can find that these two independent calculations agree very well.

Although the two methods quite consist each other, the values of the unfolding forces have apparent discrepancies with experimental measurements. For example, in the absence of Mg^{2+} the values are 13.3, 11.3 and 8.0 pN for P5ab, P5abc Δ A, and P5abc molecules for the constant extension ensemble, respectively (6). It is not strange because we do not include the effect of ionic concentration in our model. Hence we choose a reasonable ionic correction of RNA free energies (43). Unfortunately, we still do not get good results; see Table I. There are two possible causes leading to such discrepancies. One is that the ionic corrections or free energy parameters for RNA are not precise enough; they cannot be used in the force unfolding cases. The other is that polymer elastic parameters are not very precise. We prefer to the later. In addition to RNA free energy measured and tested for almost forty years, the persistent length of ssDNA in ionic environment is still debatable (45). For instance, we calculate the unfolding forces of the three molecule with $P_{ss} = 2.2$ nm and indeed find that they are closer to the experimental values. As a further demonstration, we also list other values measured in previous experiments and compare them with theoretical predictions in the same table.

B. Single RNAs kinetics

1. Constant extension ensemble

Force-extension curves. As an example, we stretch P5ab molecule with the velocity $v = 5 \times 10^{-3} \text{ \AA}$ from the offset $z_o = 350$ nm to $z(t) = 450$ nm, and then relax it with the same velocity; here we let $\tau_o = 1$. One of the time trajectories is showed in Fig. 3A. Apparently, the

TABLE I The unfolding forces f_u of different molecules under different experimental conditions. The experimental data are from the previously published data (6; 9; 44). The theoretical values are from the exact numerical methods developed above, where f_u^i , $i = 1, 2, 3$ represent the unfolding forces without the ionic correction, with the ionic correction on the free energy and with the ionic and the persistent length corrections, respectively. Here We do not show the P5abc unfolding force for it is not reversible in Mg^{2+} due to the presence of tertiary interactions.

Molecule	temperature (K)	Na^+ (mM)	Mg^{2+} (mM)	f_u^1 (pN)	f_u^2 (pN)	f_u^3 (pN)	f_u^{exp} (pN)
P5abc	298	250	0	12.2	11.4	10.0	7.0-11.0
poly(dA-dU)	293	150	0	12.3	11.0	9.3	9.0
P5abc Δ A	298	250	0	15.8	14.8	13.2	11.4 ± 0.5
P5abc Δ A	298	250	10		15.4	13.8	12.7 ± 0.3
P5ab	298	250	0	18.4	17.4	15.7	13.3 ± 1.0
P5ab	298	250	10		18.0	16.2	14.5 ± 1.0
CG hairpin	293	150	0	25.8	24.4	22.4	17.0
poly(dC-dG)	293	150	0	25.1	23.8	21.7	20.0

unfolding and refolding trajectories are not coincident, i.e., force-hysteresis, which indicates that the molecule is driven from thermodynamic equilibrium (6) occurs.

In experiments record of the force and extension at given times with a slow velocity is a more common method in the equilibrium measurement. Hence we simulate the three curves with the two slow velocities $1 \times 10^{-4} \text{ \AA}$ and $1 \times 10^{-5} \text{ \AA}$. Because enormous data would be generated if the time trajectories were recorded, we only show the data per unit times 10^5 and 10^6 (see Figs. 3C and D). For the faster velocity, we find that, except P5ab case, the unfolding forces for the others do not equal the equilibrium values; whereas for the later, the curves of simulations consist with the exact curves. It means that the unfolding of the three molecules with $1 \times 10^{-5} \text{ \AA}$ is or near equilibrium. Two features in Fig. 3D are of our interest. Compared with the curves obtained by the time averaging, the curves recorded at time points are very rough even before and after the unfolding. And although the whole extension $z(t)$ monotonically increases with time, the extensions of the molecules may still jump between two values, such as P5ab and P5abc molecules. Indeed similar phenomena were also observed in the experiment (6). They indicate the fluctuations of the extension and RNA structures under the force. Just because of this observation, and that the phenomena are not rare in simulation and the experiment.

In the experiment (6; 7), the unfolding P5abc are near-equilibrium and far from equilibrium at the loading rates 2-5 pN/s and 34-52 pN/s, respectively (similar values for P5abc Δ A). And our simulations also show that the unfolding the same molecule are near-equilibrium and far from equilibrium at the velocities 10^{-5} \AA and 10^{-4} \AA , respectively. Let them be equal correspondingly we then can estimate the constant $\tau_o \approx 10^{-7} \text{ s}$. We will scale the time with this parameter below for convenience.

Fig. 4 shows 100 trajectories with two loading rates for P5ab and P5abc molecules. The trajectories are stretched from the same offset $z_o = 350 \text{ nm}$ after ther-

mal equilibrium until the terminal extension $z = 450 \text{ nm}$. For both the loading rates, below and above the unfolding forces, the force-extension curves are dominated by the double-stranded handles. But the values of the unfolding forces apparently fluctuate and dependent on the rate and the molecular type. When the pulling speed is faster, or the loading rate is larger (1000 pN/s), the average unfolding force increases correspondingly. This phenomenon has been theoretically predicted earlier (46). We note that at the same loading rate, the trajectories of P5ab are closer to its equilibrium force-extension curve than the trajectories of P5abc. It means that the relaxing process of the former is faster than the latter. This fact has also been observed in the experiment (6).

Free energy reconstruction. According to Ref. (47), the unperturbed molecular free energy landscape $G_o(x)$ along the molecular extension x can be calculated from position-versus-time curves with the expression

$$G_o(x) - G(t=0) = -\beta^{-1} \log \langle \delta(x - x(t)) \exp(\Delta w_t) \rangle \quad (14)$$

where $\Delta w_t = w_t - k_{tw}(x(t) - vt)^2/2$, $G(t=0)$ is the free energy of the whole system in equilibrium at initial time $t = 0$, and

$$w_t = k_{tw}v(vt^2/2 + z_o t - \int_0^t x(t') dt') \quad (15)$$

The free energy landscape can be reconstructed by one time slice according to Eq. 14. But considering that for finite stretching trajectories, we only sample a small window around the molecular equilibrium position at the whole extension $z(t)$, Therefore, a weighted histogram method was proposed (47),

$$G_o(x) - G(t=0) = -\beta^{-1} \log \frac{\sum_{t_i} \frac{\langle \delta(x - x_i) \exp(-\beta w_{t_i}) \rangle}{\langle \exp(-\beta w_{t_i}) \rangle}}{\sum_{t_i} \frac{\exp[-\beta u(x(t_i), t_i)]}{\langle \exp(-\beta w_{t_i}) \rangle}}, \quad (16)$$

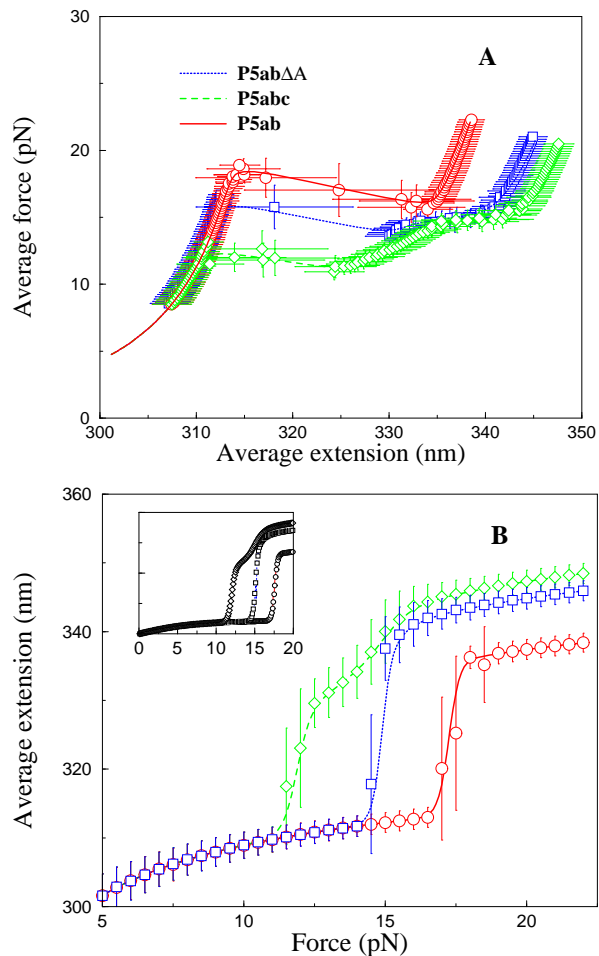


FIG. 2 Comparison of the exact and simulation force-extension curves in equilibrium for P5ab, P5abc Δ A and P5abc on the constant extension (A) and the constant force (B) ensembles. The different symbols are from the simulation methods, and the different lines are from the exact methods. They agree with each other very well. Inset, force-extension curves for the same ensemble recalculated by another move set.

where the sum is over many time slices t' , and the average is over the repeated trajectories at each given time slice. For each trajectory, we choose the discrete time $t_i = i\Delta t$, $i = 1, \dots, 100$, here $\Delta t = 10/v$, i.e., the time moving the light trap 1 nm (or every point in Fig. 4).

Fig. 5 shows the finally reconstructed free energy landscapes for the two molecules at two loading rates 20 and 40 pN/s. The precisions of reconstructions are satisfactory. We note that landscapes are unexpectedly trivial: neither of them presents energy barrier. Ref. (48) has investigated Jarzynski's equality by modelling RNA molecules as a two-level system with an intermediate barrier. Our calculations apparently contradict their assumption. Indeed, the strong unfolding-refolding cooperativity observed in the experiments (6; 7) arises from the coupling of the RNA molecules and the light trap;

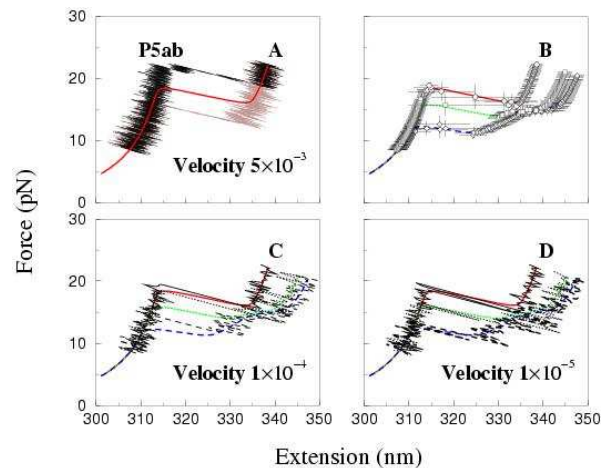


FIG. 3 A. One of the time trajectories of unfolding and refolding for P5ab with velocity $5 \times 10^{-3} \text{ \AA}$. Force-hysteresis is observed. B. Fig. 2A is showed here again. C. The unfolding force-extension curves recorded at unit time 10^5 for the molecules with velocity $1 \times 10^{-4} \text{ \AA}$. D. The force-extension curves recorded at time unit 10^6 with velocity $1 \times 10^{-5} \text{ \AA}$.

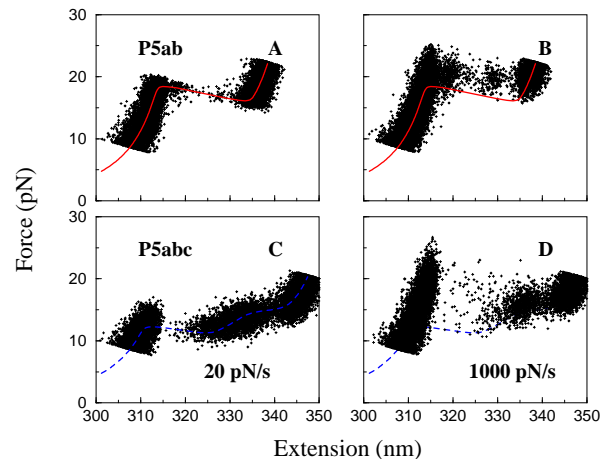


FIG. 4 Unfolding trajectories of P5ab (A,B) and P5abc (C,D) with loading rates 20 and 1000 pN/s. Curves (superposition of 100 curves per figure) are represented by 100 points with the equal time interval; for clarity we do not connect them with lines.

the addition of their potentials is a two-level system (see the respective insets in the figure). Therefore, the two-level system, although is a good approximation in RNA folding study, should not be simply copied to the force unfolding cases.

Free Energy Difference Estimators Although Jarzynski's equality has many applications, our understanding of its behavior is still rather limited (49). For example, we are not clear whether other free energy estimators are better than the equality, and whether the number of repeated trajectories in landscape reconstruc-

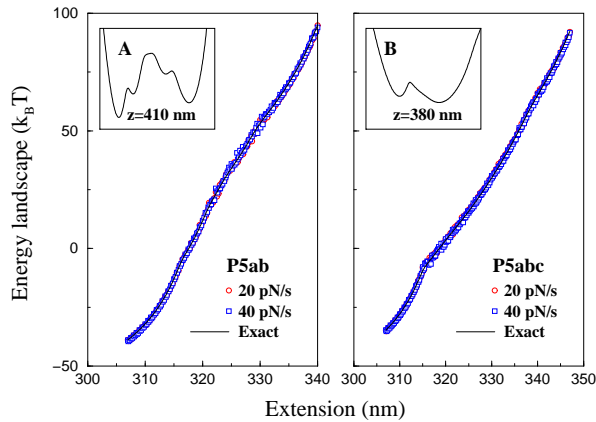


FIG. 5 Comparison of the free energy landscapes of the two molecules P5ab and P5abc reconstructed from the Jarzynski equality with two loading rates 20 and 40 pN/s and the exact landscapes calculated from the partition function method. The number of trajectories for each case is 1000. The insets are the free energy landscapes of the system composed of the molecules and the light trap potential, which are from partition function method. Note that we do not show the scales of the extensions and free energies.

tion above is enough or excessive to achieve reasonable precisions. Recently such discussions have attracted considerable interests (49; 50; 51). Our simulation here provides a good opportunity to numerically investigate these questions.

Instead of the molecular free energies, we will use the systematic free energies (the molecule and the optical trap) for simplicity. Hence we define Jarzynski estimator $\Delta G_{JE}(z) = -\beta^{-1} \log \langle \exp(-\beta w_z) \rangle_N$ (we here replace time t by the whole extension z because of the linear relation between them) and $\Delta G_{JE}(z) = G_{JE}(z) - G_{JE}(z_0)$. Two other common estimators that can be used to calculate the free energy differences are the mean work estimator $\Delta G_{MW}(z) = \langle w_z \rangle_N$ and the fluctuation-dissipation theorem estimator $\Delta G_{FD}(z) = \langle w_z \rangle_N - \beta \sigma_w^2$, where σ_w is the standard deviation of the work distribution (52).

To get an intuitive observations about the three estimators, we calculate the free energy differences between the estimators and the exact energies, $\Delta G_i(z) - \Delta G(z)$, $i = MW, FD$, and JE . The differences of P5ab and P5abc with the loading rates 20 and 40 pN/s respectively are showed in Figs. 6A and B; here we choose $N=1000$.

There are two common features in the figure. First is that the free energy differences for each estimator are not uniform along the distance. For example for JE estimator, the differences are maximum around the unfolding distances such as 415 nm for P5ab. Therefore we conclude that nonequilibrium behaviors of the same molecule are not uniform along its extension, even if the RNA is unfolded with the same loading rate. Then for both the molecules, the JE estimator is always better than the MW at any loading rates. For the P5ab case, the FD

estimator is more or less better than the JE as the extension $z > 415$ nm. This trend is more apparent as P5ab is unfolding with smaller loading rate 20 pN/s. In contrast, the JE estimator for P5abc is superior to the FD estimator over the entire extension range at the two loading rates.

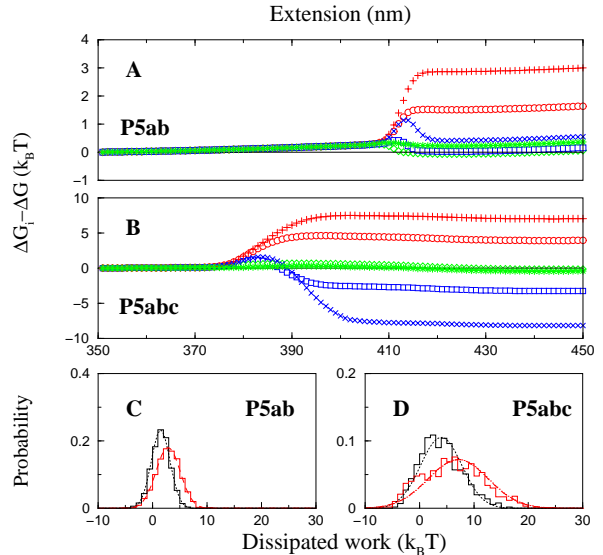


FIG. 6 A and B. The differences between the three free energy estimators and the exact energies for P5ab and P5abc at two loading rates 20 (closed symbols) and 40 pN/s (crossed symbols): MW circle and plus, FD square and times, and JE diamond and star. Here $N=1000$. C and D. Histograms of the dissipated works at extension $z = 430$ nm for P5ab and P5abc molecules at the two loading rates. The lines are Gaussian functions with mean and variance from the same data, where the dotted lines are for 20 pN/s, and the dashed lines are for 40 pN/s.

Because the above analysis is carried out at a given N -value, we do not consider the errors caused by different samples. In addition, we also do not consider how the results depend on the number of trajectories. Ref. (49) has studied the issues in two extreme situations: the large N limit and the system in the near-equilibrium regime. Because of $N \leq 100$ in the current real experiment, in the present work we investigate them in the middle value of N , although it is not hard to run 10^5 trajectories in our simulation “experiment”. Previous analysis has found that different from the case far from equilibrium, the properties of the three estimators in the near-equilibrium regime are independent of concrete models. Hence the investigation should provide a good opportunity to test the correctness of the unfolding kinetics we designed.

Ref. (49) has introduced three important properties associated with the estimators: bias $B_i(z) = \langle \Delta G_i(z) - \Delta G(z) \rangle$, which represents systematic error created by the finite N ; variance $\sigma_i^2(z) = \langle (\Delta G_i(z) - \langle \Delta G_i(z) \rangle)^2 \rangle$ accounting for statistical error because of different samples, and mean square error (MSE), a standard measure for the

quality of an estimator, $MSE_i(z) = \sigma_i^2(z) + B_i^2(z)$, where $i = \text{MW, FD and JE}$. Although these quantities depend on the distance z , we choose a representation at $z = 430$ nm for simplifying the discussion below: when the extension z is greater than the unfolding distance, the qualitative behaviors of the quantities are almost the same. The biases and variances dependence on N for the JE estimators for P5ab and P5abc are plotted in Fig. 7A and B, and the MSEs dependence on N for the three estimators are in Fig. 7C and D, where two loading rates are 20 and 40 pN/s, respectively, and each symbol is the average of 100 sets.

For P5ab case, we note that both the biases and variances of the JE estimator at the two loading rates can be well approximated with power functions. For example, at the loading rate 20 pN/s, the bias $B_{JE}(430) = \langle w_{dis} \rangle(430)/N^\alpha = 1.57/N^{0.55}$, and $\sigma_{JE}^2(430) = \sigma_w^2/N^\gamma = 2.86/N^{0.65}$, where the dissipated work $w_{dis}(z = 430)$ is defined as $w_z - \Delta G(z)$, and $\sigma_w^2 = \langle (w_z - \langle w_z \rangle)^2 \rangle$; they also are the bias and variance of the JE estimator with $N = 1$. This interesting observation can be understood from the distributions of the dissipated works. Fig. 6C shows their histograms. We find that they both agree well with Gaussian functions whose means and variances are obtained from the corresponding data. Indeed, according to the force-extension curves, we argued that the unfolding of P5ab at loading rate 20 pN/s is near-equilibrium; see Fig. 3A. The good agreement between the histograms and Gaussian function therefore is not unexpected: when a system is in the near-equilibrium regime, it always have a Gaussian dissipated work distribution, and in particular, an important equality holds, $\sigma_w = 2\beta^{-1}\langle w_{diss} \rangle$ (52); here $2.86 \approx 2 \times 1.57$. Another demonstration of P5ab in the near-equilibrium regime is that the MSEs of the three estimators obtained by our simulations consist with the following expressions (49; 51):

$$\begin{aligned} MSE_{MW} &= 2\frac{\langle w_{dis} \rangle}{\beta N} + \langle w_{dis} \rangle^2 \\ MSE_{FD} &= 2\frac{\langle w_{dis} \rangle}{\beta N} + 2\frac{\langle w_{dis} \rangle^2}{N-1} \\ MSE_{JE} &= 2\frac{\langle w_{dis} \rangle}{\beta N^\gamma} + \frac{\langle w_{dis} \rangle^2}{N^{2\alpha}}; \end{aligned} \quad (17)$$

see the lines in Fig. 7C. We firstly see that MW estimator is the worst among the three estimators. Although it is known that the FD estimator in near-equilibrium regime is unbiased, for smaller N , here about ≤ 10 , the JE estimator is still superior to FD. This result is from the error in estimating σ_w^2 from limited data. When N is larger, FD estimator is the best among them. Our observations are coincident with the previous analysis (49). In addition, we also see that for the case of 40 pN/s, larger number of trajectories will be required to get the same quality of any estimator.

So how about the estimators far from equilibrium? The same properties are showed in Fig. 7B and D. We see

that at the loading rates we presented, although the variances can still be approximated with power functions, e.g., $\sigma_{JE}^2(430) = 13.46/N^{0.9}$ for P5abc at 20 pN/s, no such functions present in the biases. The discrepancies of the histogram and the Gaussian function of P5abc in Fig. 6D also reflect it. Even if no analytic results have been obtained except the large N limit (49; 50), our simulations still give some hints about the properties of the three estimators in the far-from-equilibrium regime: JE estimator should be the best among the estimators; while FD and MW estimators be almost equally poor in this regime.

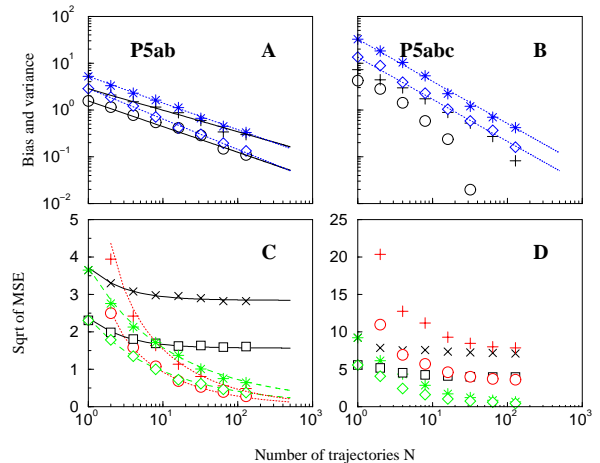


FIG. 7 A and B. Biases and variances dependence on the number of trajectories for P5ab and P5abc molecules at two loading rates 20 (closed) and 40 pN/s (crossed) at the extension $z = 430$ nm. C and D. Square roots of the MSEs for the three estimators for the two molecules at the same extensions: MW estimator square, times and solid line; FD estimator circle, plus and dotted line; and JE estimator diamond, star and dashed line.

2. Constant force ensemble

Compared to the general thermodynamics of RNA under force in equilibrium, single-molecule methods are more interesting in kinetic folding and unfolding studies. With the single molecule experiments we can follow the actual folding or unfolding trajectories of a single molecules on high resolution even when they occur in equilibrium state, which will shed light on the difficult kinetic folding problem (28; 29). We mentioned above that the extension of P5ab in the constant extension ensemble may hop back and forth between two states. To investigate this bistability, Ref. (6) imposed a constant force on P5ab (6). They found that, when the force was held constant at the transition within ~ 1 pN, P5ab switched back and forth with time from the folded hairpin (hp) to the unfolded single strand (ss). A two-state kinetics was proposed to explain the intrigu-

ing phenomenon. The rate constants for unfolding reaction can be fit to an Arrhenius-like expression of the form $k_u(f) \propto \exp(f\Delta x_u^\ddagger/k_B T)$, where Δx_u^\ddagger is the thermally averaged distance between the hairpin state and the transition state along the direction of force. A similar expression also holds for the folding rate $k_f(f)$. Apparently, this description can not clarify the physics underlying the folding and unfolding reactions.

Because our simulation is based on the microscopic interactions, we are interested in whether the similar time traces can be obtained by simulation. We are not ready to choose the direct move sets in Eq. 1, instead another reasonable move set was proposed (28) to enhance simulation efficiency. Because what we concern about is kinetic behaviors of single RNA, for convenience the contribution of double-stranded handles is neglected. Indeed, under constant force the handle can be viewed as one part of the feedback mechanism. If we model single-stranded part of RNA structure S_i as an extensible freely joined chain, the elastic free energy contribution of it under force f then is $W^{ss}(n_i, f) = n_i k_B T b_{ss} / P_{ss} \ln [\sinh(u)/u]$, where $u = l_{ss} f / k_B T$. Therefore Eq. 2 is largely simplified in such ensemble as

$$\Delta G_i^0 - W^{ss}(n_i, f). \quad (18)$$

We see that the extensional variables are absent from systematic energy. Note the extension we record in simulation now is $x_{ss}(f, n_i)$. Such simplification requires that under mechanical force the conformational relaxation process of the single stranded part of RNA is faster than the slowest process of the secondary structural arrangement. Our discussion shows that in contrast to the constant extension ensemble, the RNA secondary structure S alone can completely specify any state of the constant force ensemble. Therefore, the move set is the same with the set for RNA folding without force, i.e., the unfolding space is $C(l)$.

we recalculate the force-extension curves for the three RNA molecules in equilibrium; see Fig. 2 inset. Except the regions before transitions where the elastic property of the handle dominates, the shapes of the curves and the values of unfolding force obtained by the two different simulation methods are almost the same.

We record the extension-time traces of the RNA molecules at different constant forces in equilibrium. In order to compare with real data, ionic correction are took into account (see the third corrections in Table I). For example, one extension-time traces at force 14.8 pN for P5ab without Mg^{2+} is shown in Fig. 8A. The extension of the molecule jumps between two values, ~ 5 nm and ~ 22 nm around the unfolding force. Because the jumps are extremely rapid with respect to the lifetimes of the molecule in the two states, we simply classify the states whose extensions are larger than 15 nm as the single stranded states, and the others as the hairpin states. In addition, there are significant fluctuations about the two states. Around the unfolding the frequencies of the different lifetimes at the single stranded state and the

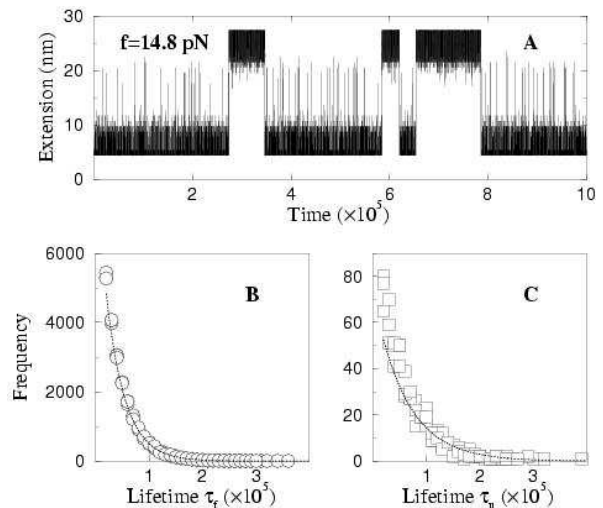


FIG. 8 Simulation for RNA p5ab kinetics. A. Extension versus time traces of the molecule at a force in equilibrium, here the unit of time is τ_o . Frequency distributions of the lifetimes of the single stranded (B) and hairpin states (C) at 14.2 pN. The average lifetimes of these two states in this simulation can be obtained by fitting to exponential functions; see the curves therein.

hairpin state can be obtained by a long time simulation (in order to get enough data, the simulation time is $10^9 \tau_o$ after equilibrium). Fig. 4c shows the frequency distributions of a typical simulation at force 14.2 pN. These distributions can be fit to an exponential function $\propto \exp(-t/\langle\tau_i\rangle)$ very well, where $\langle\tau_i\rangle$, $i = u, f$ denote the force-dependent average lifetimes at the two states, respectively. For example, the average lifetimes in this simulation are $\langle\tau_u\rangle \approx 6.2 \times 10^4 \tau_o$ and $\langle\tau_f\rangle \approx 3.5 \times 10^4 \tau_o$. We calculate all average lifetimes near the unfolding force of P5ab, and their corresponding values with different forces are shown in Fig. 9. We find that the logarithms of the lifetimes for the two states are strikingly consistent with linear functions of the forces. Because the reaction rate constants are the inverse of the average lifetimes, we fit τ_o by making $\langle\tau_u\rangle(f^*) = \langle\tau_f\rangle(f^*)$ equal to the experimental value $1/k^*$, where $k^* \equiv k_u = k_f$, and had $\tau_o^{-1} = 2.6 \times 10^5 \text{ sec}^{-1}$. Using the same method, the reaction rate constants for P5ab in the presence of Mg^{2+} are also calculated. A comparison of the simulation results and the experimental data is listed in Table II. Because our simulation does not need additional fitting parameters, the striking consistence of our results with the experiment assures us that the RNA folding and unfolding model proposed here has grabbed the main physics.

IV. DISCUSSION AND CONCLUSION

Compared to the enormous kinetic simulations of the force unfolding proteins, the effort contributed to RNA is relatively little. To fit the gap, we developed a kinetic

TABLE II Simulation results for P5ab compared to the experimental data from Ref. (6) (in bold).

Molecule	$\langle \Delta x \rangle (nm)$	$f^* (pN)$	$\ln k_f(f)(s^{-1})$	$\ln k_u(f)(s^{-1})$
P5ab, Mg^{+2}	19 ± 2	14.5 ± 1	$41 \pm 1.9 - (2.8 \pm 0.1)f$	$-39 \pm 2.3 + (2.9 \pm 0.2)f$
P5ab, by Cocco et al.		15.1	$27.5 - 2.74f$	$-42.9 + 1.93f$
P5ab, by us	20.0	14.7	$39.4 - 2.6f$	$-30.1 + 2.2f$
P5ab, EDTA	18 ± 2	13.3 ± 1	$37 \pm 4.0 - (2.7 \pm 0.3)f$	$-32 \pm 4.8 + (2.6 \pm 0.4)f$
P5ab, by us	20.0	14.2	$35.7 - 2.4f$	$-28.3 + 2.1f$

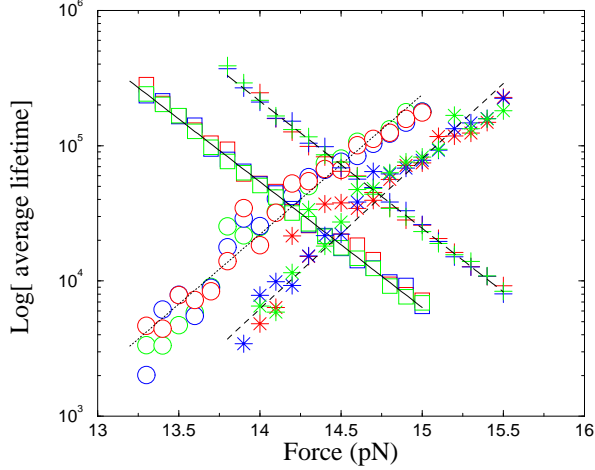


FIG. 9 Logarithm of the average lifetimes of single stranded and hairpin states for p5ab molecule at difference forces around the unfolding. The time is in unit τ_o , which can be obtained by fitting to experimental data. Note the slopes of $\ln\langle\tau_f\rangle$ and $\ln\langle\tau_u\rangle$ are independent of the fitting value τ_o . The crossed symbols are for the presence of Mg^{2+} .

stochastic simulation to the force unfolding single RNAs. Different from previous force unfolding method, for the constant extension ensemble external time-dependent force can be taken into account correctly. We make use of the algorithm to investigate the experiment testing the important Jarzynski's equality (7). Instead of the force versus extension trajectories used in the experiment, the extension versus time trajectories are used to reconstruct the free energy landscapes, compare the qualities of the three estimators, and investigate the estimators dependence on the trajectories number. For the constant force ensemble, we particularly studied the interesting extension-time traces dependence on force, which would be relevant to RNA folding dynamics.

The most advantage in study of force unfolding RNAs is that the knowledge accumulated in the past forty years for RNA secondary structure provides a solid fundament for theoretical predictions (including kinetics and thermodynamics) in practice. Therefore, we believe that our model would be useful in RNA biophysical studies in the future. Of course several improvements

still can be added in our algorithm, e.g., adding the effects of Mg^{+2} to include complicated tertiary interactions (8). Recent works have shown that the inclusion of pseudoknots is possible (53; 54).

The computation of this work was performed on the HP-SC45 sigma-X parallel computer of ITP and ICTS, CAS. We thank Dr. Flamm for providing us his computer program KINFOLD. F.L. thanks Dr. F.Ye, R.-L. Dai, and Y. Zhang for their supporting in the computation. This research was supported by the theoretical physics special fund, NSFC.

References

- [1] Cech TR. The Chemistry of Self-Splicing RNA and RNA Enzymes. *Science* 1987;236:1532-9.
- [2] Cech TR. Structure and Mechanism of the Large Catalytic RNAs: Group I and Group II Introns and Ribonuclease P. In: Gesteland RF and Atkins JF, editors. In the RNA world. Cold Spring Harbor (NY): Cold Spring Harbor Laboratory Press; 1993. p. 239-269.
- [3] Couzin J. Small RNAs Make Big Splash. *Science* 2002;298:2296-7.
- [4] Essevaz-Roulet B, Bockelmann U, and Heslot F. Mechanical Separation of the Complementary Strands of DNA. *Proc. Natl. Acad. Sci. USA* 1997;94:11935-11940.
- [5] Harlepp S, Marchal TM, Robert J, Leger JF, Xayaphoummine A, Isambert H, and Chatenay D. *Eur. Phys. J. E* 2003;12:605-613.
- [6] Liphardt J, Onoa B, Smith SB, Tinoco I, and Bustamante C. Reversible Unfolding of Single RNA Molecules by Mechanical Force. *Science* 2001;292:733-737.
- [7] Liphardt J, Dumont BS, Smith SB, Tinoco I, and Bustamante C. Equilibrium Information from Nonequilibrium Measurements in an Experimental Test of Jarzynski's Equality. *Science* 2002;296:1832-1835.
- [8] Onoa B, Dumont S, Liphardt J, Smith SB, Tinoco I, and Bustamante C. Identifying Kinetic Barriers to Mechanical Unfolding of the T. thermophila Ribozyme. *Science* 2003;299:1892-1895.
- [9] Rief M, Clausen-Schaumann H, and Gaub HE. Sequence-dependent mechanics of single DNA molecules. *Nat. Struct. Biol.* 1999;6:346-349.
- [10] Smith SB, Cui Y, and Bustamante C. Overstretching B-DNA: The Elastic Response of Individual Double-Stranded and Single-Stranded DNA Molecules. *Science* 1996;271:795-799.

- [11] Wang MD, Yin H, Landick R, Gelles J, and Block SM. Stretching DNA with optical tweezers. *Biophys. J.* 1997;72:1335-1346.
- [12] Tinoco I and Bustamante C. How RNA Folds. *J. Mol. Biol.* 1999;293:271-281.
- [13] Hofacker IL, Fontana W, Stadler PF, Bonhoeffer S, Takcer M, and Schuster P. Fast Folding and Comparison of RNA Secondary Structures. *Monatsh. Chem.* 1994;107:2903-2912.
- [14] McCaskill JS. The Equilibrium Partition Function and Base Pair Binding Probabilities for RNA Secondary Structure. *Biopolymer* 1993;29:1105-1119.
- [15] Zuker M and Stiegler P. Optimal Computer Folding of Larger RNA Sequences Using Thermodynamics and Auxiliary Information. *Nucleic Acids Res.* 1981;9:133-148.
- [16] Montanari A and Mezard M. *Phys. Rev. Lett.* 2001;86:2178-2181.
- [17] Zhou H, Zhang Y, and Ou-Yang ZC. *Phys. Rev. Lett.* 2001;86:356-9.
- [18] Zhou H, Zhang Y, and Ou-Yang ZC. Pulling hairpinned polynucleotide chains: Does base-pair stacking interaction matter? *J. Chem. Phys.* 2001;114:8694-8700.
- [19] Muller M. Statistical physics of RNA folding. *Phys. Rev. E* 2002;67:021914-021930.
- [20] Gerland U, Bundschuh R, and Hwa T. Mechanically Probing the Folding Pathway of Single RNA Molecules. *Biophys. J.* 2003;84:2831-40.
- [21] Lubensky DK and Nelson DR. Single molecule statistics and the polynucleotide unzipping transition. *Phys. Rev. E* 2002;65:031917-031941
- [22] Liu F, Dai LR, and Ou-Yang ZC. Theory for the force-stretched double-stranded chain molecule. *J. Chem. Phys.* 2003;119:8112-8123.
- [23] Rief M, Fernandez JM, and Gaub ME. Elastically coupled two-level systems as a model for biopolymer extensibility. *Phys. Rev. Lett.* 1998;81:4764-7.
- [24] Lu H, Israelewitz B, Krammer A, Vogel V, and Schulten K. Unfolding of Titin Immunoglobulin Domains by Steered Molecular Dynamics Simulation. *Biophys. J.* 1998;75:662-671.
- [25] Bryant Z, Pande VS, and Rookhsar DS. Mechanical Unfolding of a beta -Hairpin Using Molecular Dynamics. *Biophys. J.* 2000;78:584-589.
- [26] Klimov DK and Thirumalai D. Stretching single-domain proteins: Phase diagram and kinetics of force-induced unfolding *Proc. Natl. Acad. Sci. USA* 1999;96:6166-6172.
- [27] Socci ND, Onuchic JN, and Wolynes PG. Stretching lattice models of protein folding. *Proc. Natl. Acad. Sci. USA* 1999;96:2031-5.
- [28] Liu F and Ou-Yang ZC. Unfolding single RNA molecules by mechanical force: a stochastic kinetic method. *Phys. Rev. E* 2004;70:0409011-4.
- [29] Liu F and Ou-Yang ZC. Monte carlo Simulation for Single RNA Unfolding by Force. *Biophys. J.* 2005;88:76-84.
- [30] Jarzynski C. Equilibrium equality for free energy differences. *Phys. Rev. Lett.* 1997;78:2690-2693.
- [31] Liu F and Ou-Yang ZC. Force unfolding single RNAs and Jarzynski's equality. Submitted.
- [32] Gulyaev AP, van Batenburg FHD, and Pleij CWA. The Computer Simulation of RNA Folding Pathways Using a genetic Algorithm. *J. Mol. Biol.* 1995;250:37-51.
- [33] Mironov A. and Lebedev VF. A Kinetic Model of RNA Folding. *Biosystems* 1993;30:49-56.
- [34] Flamm C, Fontana W, Hofacker I, and Schuster P. RNA Folding at Elementary Step Resolution. *RNA* 2000;6:325-338.
- [35] Breton N, Jacob C, and Daegelen P. Prediction of Sequentially Optimal RNA Secondary Structures. *J. Biomol. Struct. Dyn.* 1997;14:727-740.
- [36] Bustamante C, Marko JF, Siggia ED, and Smith SB. Entropy elasticity of lambda-phage DNA. *Science* 1994;265:1599-1600.
- [37] Bortz AB, Kalos MH, and Lebowitz JL. A New Algorithm for Monte Carlo Simulation of Ising Spin Systems. *J. Comput. Phys.* 1975;17:10-18.
- [38] Gillespie DT. Markov Process: an Introduction for physical Scientists. San Diego, California: Academic Press; 1992.
- [39] Jansen APJ. *Comp. Phys. Commu.* 1995;86:1-12.
- [40] Press WH, Teukolsky SA, Vetterling WT, and Flannery BP. Numerical Recipes in C: the Art of Scientific Computing. Cambridge, England: Cambridge University Press; 1992.
- [41] Kawasaki K. Diffusion Constants near the Critical Point for Time-dependent Ising Models. *Phys. Rev.* 1966;145:224-230.
- [42] Hofacker IL. The Vienna RNA Secondary Structure Server. *Nucl. Acids. Res.* 2003;31:3429-3431.
- [43] Cocco S, Marko JF, and Monasson R. Slow Nucleic Acid Unzipping Kinetics from Sequence-defined Barriers. *Eur. Phys. J. E* 2003;10:153-161.
- [44] Bustamante C, Smith SB, Liphardt J, and Smith D. Single-molecule studies of DNA mechanics. *Curr. Opin. Struct. Biol.* 2000;10:279-285.
- [45] Murphy MC, Rasnik I, Cheng W, Lohman TM, and Ha T. Probing Single-Stranded DNA Conformational Flexibility Using Fluorescence Spectroscopy. *Biophys. J.* 2004;86:2530-7.
- [46] Evans E and Ritchie K. Dynamic Strength of Molecular Adhesion Bonds. *Biophys. J.* 1997;72:1541-1555.
- [47] Hummer G and Szabo A. Free energy reconstruction from nonequilibrium single-molecule pulling experiments. *Proc. Natl. Acad. Sci. USA* 2001;98:3658-3661.
- [48] Ritort F, Bustamante C, and Tinoco I. A Two-state Kinetic Model for the Unfolding of Single Molecules by Mechanical Force. *Proc. Natl. Acad. Sci. USA* 1997;99:13544-8.
- [49] Gore J, Ritort F, and Bustamante C. Bias and error in estimates of equilibrium free-energy differences from nonequilibrium measurements. *Proc. Natl. Acad. Sci. USA* 2003;100:12564-12569.
- [50] Zuckerman D and Woolf T. Theory of a systematic computational error in free energy differences. *Phys. Rev. Lett.* 2002;89:1806021-4.
- [51] Hummer GJ. Fast-growth thermodynamic integration: error and efficiency analysis. *J. Chem. Phys.* 2001;114:7330-7337.
- [52] Hermans J. Simple analysis of noise and hysteresis in (slow-growth) free energy simulations. *J. Phys. Chem.* 1991;95:9029-9032.
- [53] Isambert H and Siggia ED. Modeling RNA Folding Paths with Pseudoknots: Application to Hepatitis Delta virus Ribozyme. *Proc. Natl. Acad. Sci. USA* 2000;97:6515-6520.
- [54] Rivas E and Eddy SR. A Dynamic Programming Algorithm for RNA Structure Prediction Including Pseudoknots. *J. Mol. Biol.* 1999;285:2053-2068.